Improvement of Range Resolution of FDMAS Beamforming in Ultrasound Imaging

Ryoya Kozai, Jing Zhu, Kan Okubo and Norio Tagawa
Graduate School of System Design, Tokyo Metropolitan University, Hino, Tokyo 191-0065, Japan

Keywords: Reception Beamforming, Super-resolution, Transmission With Frequency Sweep, MUSIC Algorithm.

Abstract: Ultrasound imaging is applied to various fields because it is noninvasive and real-time imaging is possible. However, in diagnosis applications, ultrasound imaging is inferior in resolution to other modalities, so researches for improving resolution have been actively conducted. Recently, researches on beamforming methods have been advanced for the purpose of improving lateral resolution. In order to form a narrower beam, adaptive beamformers such as the MV (minimum variance) beamformer that adaptively changes the beamforming weights have been proposed, but these methods increase the computational complexity. Therefore, in recent years, the FDMAS (Filtered-Delay Multiply And Sum) beamformer which can realize high resolution and high contrast without using complicated calculation attracts attention. On the other hand, we proposed a method called the SCM (Super resolution FM-Chirp correlation Method) that improves range resolution based on frequency sweep. In addition, we proposed a new DAS (Delay And Sum) beam former which improves range resolution by multiplying the echo signal by the result of the SCM before DAS processing. This method is constructed in the usual RF (Radio Frequency) band. In this study, we first reconstruct the FDMAS as a baseband processing in order to improve the SNR, and apply the SCM result to the FDMAS in order to improve both range and lateral resolution.

1 INTRODUCTION

Ultrasound imaging is effectively used for medical diagnosis (Amy et al., 2015) and non-destructive inspection. (Ylitalo, 1996) In particular, real-time imaging is a major advantage of ultrasonic imaging, and it has been extended to applications such as an automobile obstacle detection system (Shoval and Borenstein, 2001) and an indoor positioning system. (Hazas and Hopper, 2006) Currently, researches aimed at improving the performance of ultrasonic imaging are actively conducted, and further improvements are also expected in the future.

Recent researches on the ultrasonic beamforming methods have been particularly advanced in the lateral resolution. The beamforming method serves as the basis of array signal processing using a transducer array composed of a plurality of transducer elements and is a technique to improve the lateral resolution by forming directivity. The most basic beamforming method is the DAS (Delay and Sum) (Thomenius, 1996) that compensates for the delay of received signals between transducer elements of the sensor array and adds them. However, this technique strongly reflects the limitation of the beam width determined by the aperture width of the transducer array. In order to form a narrower beam, adaptive beamformers such as the MV (Minimum Variance) beamformer (Wang et al., 2005; Vignon and Burcher, 2008; Holm et al., 2009) that adaptively changes the beamforming weights have been proposed, but these methods increase the computational complexity. Recently the FDMAS (Filtered-Delay Multiply and Sum) beamformer (Matrone et al., 2015) which can realize high resolution and contrast without complicated calculation by using approximate calculation of correlation between received signals of each transducer element attracts attention. Various extensions of the FDMAS have been proposed in (Matrone et al., 2017; Matrone et al., 2018; Su et al., 2018). On the other hand, we proposed methods called the SCM (Super-resolution FM-Chirp correlation Method) (Fujiwara et al., 2009) and the SA-SCM (Synthetic Aperture-SCM) (Wada et al., 2015; Tagawa et al., 2018) to improve the range resolution. These methods realize super resolution in the range direction by using the phase information of the carrier wave by transmitting and receiving a plurality of pulses with different carrier frequencies. The SCM utilizes focused pulse transmission and the SA-SCM is an extension of the SCM to utilized divergent

Kozai, R., Zhu, J., Okubo, K. and Tagawa, N.
Improvement of Range Resolution of FDMAS Beamforming in Ultrasound Imaging.
DOI: 10.5220/0007583601980205
In *Proceedings of the 14th International Joint Conference on Computer Vision, Imaging and Computer Graphics Theory and Applications (VISIGRAPP 2019)*, pages 198-205
ISBN: 978-989-758-354-4

pulse transmission for the purpose of increasing the frame rate. The SA-SCM transmits divergent pulses and applies the SA processing (Jensen et al., 2006), for example the DAS, as a reception beamformer to echoes received by all transducer elements. After calculating each line signal, resolution is improved by applying the SCM. Since the SCM is a processing for each image line, discontinuities tend to occur in the lateral direction. In order to solve this problem, we first applied the SCM to the received echo of each element, and multiply the received echo by the result to generate the echo signal with high range resolution. After that, by applying the DAS to the obtained high-resolution echoes, we constructed a beam former called the SCM-weighted SA, in which lateral discontinuities do not occur. (Zhu and Tagawa, 2018)

In this study, we aim to improve the lateral resolution based on the FDMAS. First, by reconstructing the FDMAS as baseband processing, it is possible to use not only the frequency band of twice the transmission frequency used in the FDMAS but also the transmission frequency band. SNR (Signal-to-Noise Ratio) is expected to be improved by using this baseband FDMAS. Since the SCM is executed in baseband, the result of the SCM can be efficiently incorporated into the baseband FDMAS. By this new beam former, in which the SCM results are used as the same way of the SCM-weighted SA. we simultaneously improve both range and lateral resolution.

2 METHOD

2.1 Super-Resolution FM-Chirp Correlation Method

In this section, we explain the principle of the SCM. We transmit a FM-chirp pulse $s(t) = \mathrm{Re}[x(t)e^{j\omega_0 t}]$ with a center frequency of ω_0, and receive the echo signal $y(t)$ in RF-band from D point scatterers, which is mathematically expressed as

$$y(t) = \int_{-\infty}^{\infty} h(\tau)s(t-\tau)d\tau, \tag{1}$$

$$h(t) = \sum_{i=1}^{D} h_i \delta(t-\tau_i), \tag{2}$$

where h_i is the set of the amplitudes of reflections in all the scatterers, τ_i is set of propagation delay times of echoes of all scatterers, and $\delta(\cdot)$ is the Dirac delta function. The received FM-chirped echo is expressed as a baseband analytic signal $v(t)$, and a compressed

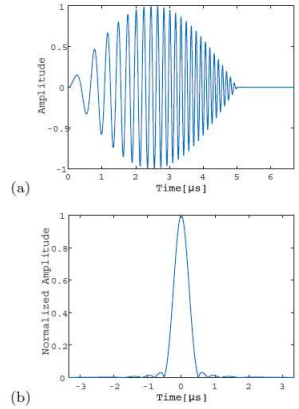

Figure 1: Example of FM-chirp pulse compression: (a) transmitted signal $s(t)$ with 8 MHz bandwidth and with Hanning window apodization; (b) absolute value of compressed signal $r(t)$.

signal is formulated as $z(t)$, which are

$$v(t) = \sum_{i=1}^{D} h_i x(t-\tau_i)e^{-j\omega_0\tau_i} + n(t), \tag{3}$$

$$z(t) = \sum_{i=1}^{D} h_i r(t-\tau_i)e^{-j\omega_0\tau_i} + m(t), \tag{4}$$

where $r(t)$ is the autocorrelation function of $x(t)$ in the baseband that takes complex values, and hence, $z(t)$ is the complex valued delay profile. The observation noise $n(t)$ is assumed to be Gaussian white noise restricted to baseband with variance σ^2, and hence, $m(t)$ is the complex value cross-correlation of $x(t)$ and $n(t)$. An example of FM-chirp pulse compression is shown in Fig. 1.

Equation 4 shows that the echo from each scatterer has a phase that depends on the carrier frequency ω_0 and the scatterer position. Therefore, by receiving echoes of different carrier frequencies, it is possible to separate scatterers based on phase information. Figure 2 shows an example of the phase information obtained by different frequency transmission.

The MUSIC (MUltiple SIgnal Classification) algorithm (Schmidt, 1986; Zhou et al., 2008) is used for super-resolution processing of the SCM. As a discrete representation, we define a compressed echo vector $\boldsymbol{z} \equiv [z(t_1), z(t_2), \cdots, z(t_M)]^\top$, a steering vector $\boldsymbol{r}_i \equiv [r(t_1-\tau_i), r(t_2-\tau_i), \cdots, r(t_M-\tau_i)]^\top$ indicating the compressed echo of the i th scatterer, and a noise vector $\boldsymbol{m} \equiv [m(t_1), m(t_2), \cdots, m(t_M)]^\top$ with M the number of time sampling. Using an array manifold matrix $\boldsymbol{\Gamma} \equiv [\boldsymbol{r}_1, \boldsymbol{r}_2, \cdots, \boldsymbol{r}_D]^\top$ and a gain vector $\boldsymbol{g} \equiv [h_1 e^{-j\omega_0\tau_1}, h_2 e^{-j\omega_0\tau_2}, \cdots, h_D e^{-j\omega_0\tau_D}]^\top$, $\boldsymbol{z}$ and its variance covariance matrix $\boldsymbol{R}$ can be formulated as

$$\boldsymbol{z} = \boldsymbol{\Gamma}\boldsymbol{g} + \boldsymbol{m}, \tag{5}$$

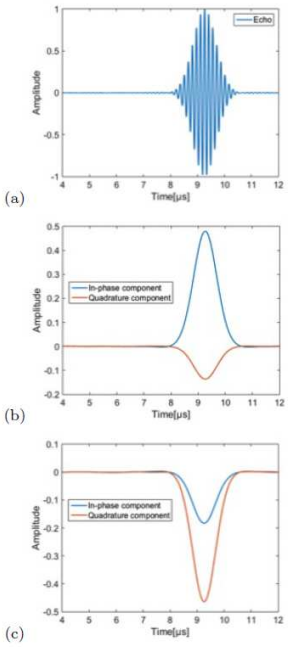

Figure 2: Phase information obtained by transmitting multiple pulses having different frequencies: (a) example of compressed FM-chirp echo; (b) I (In-phase) and Q (Quadrature-phase) components of z corresponding to (a); (c) I and Q components for different frequency transmission.

$$\boldsymbol{R} = \boldsymbol{\Gamma} \boldsymbol{G} \boldsymbol{\Gamma}^{\top} + \boldsymbol{R}_n, \tag{6}$$

$$\boldsymbol{G} \equiv E_{\omega_0}[\boldsymbol{g}\boldsymbol{g}^{\mathrm{H}}], \tag{7}$$

$$\boldsymbol{R}_n \equiv E_n[\boldsymbol{m}\boldsymbol{m}^{\mathrm{H}}] = \sigma^2 \boldsymbol{R}_0, \tag{8}$$

where $E_{\omega_0}[\cdot]$ and $E_n[\cdot]$ indicate the expectation operators with respect to ω_0 and $E_n[\cdot]$ and with respect to $n(t)$ respectively by assuming that echoes and observation noise are statistically independent. The Hermitian matrix $\boldsymbol{R}_0$ consists of $r(t)$, and the (k,l)th element is $r(t_k - t_l)$. The superscript H means complex conjugate transpose. In the SCM processing, it is necessary to solve the generalized eigenvalue problem of the following equation to obtain eigenvalues λ_i and eigenvectors $\boldsymbol{e}_i$.

$$\boldsymbol{R}\boldsymbol{e}_i = \lambda_i \boldsymbol{R}_0 \boldsymbol{e}_i, \qquad i = 1, 2, \cdots, M. \tag{9}$$

When $M > D$, the column vectors of $\boldsymbol{\Gamma}$ are linearly independent, and hence, the rank of $\boldsymbol{R} - \boldsymbol{R}_n = \boldsymbol{\Gamma}\boldsymbol{G}\boldsymbol{\Gamma}^{\mathrm{H}}$ is D. Therefore, $\boldsymbol{R}$ has D generalized eigenval ues greater than σ^2 and $M - D$ generalized eigenvalues equal to σ^2. The set of D eigenvectors $\{\boldsymbol{e}_i\}_{i=1}^{D}$ corresponding to the largest D eigenvalues spans the signal subspace. The remaining $M - D$ eigenvectors $\{\boldsymbol{e}_i\}_{i=D+1}^{M}$ span the noise subspace that does not contain signals. The noise subspace is orthogonal to the steering vector corresponding to the true delay time of the echo.

In order to estimate the arrival time of the reflected wave from the scatterer, the orthogonality between the steering vector and the noise subspace is evaluated by changing the delay time of the steering vector as a super-resolution delay profile $S(t_i)$ defined as

$$S(t_i) \equiv \frac{\boldsymbol{r}_i^{\mathrm{H}} \boldsymbol{R}_0^{-1} \boldsymbol{r}_i}{\sum_{j=D+1}^{M} |\boldsymbol{r}_i^{\mathrm{H}} \boldsymbol{e}_j|^2}. \tag{10}$$

If t_i matches the actual position of the scatterer, the corresponding $\boldsymbol{r}_i$ is orthogonal to $\{\boldsymbol{e}_j\}_{j=D+1}^{M}$, and hence, the denominator of Eq. 10 becomes small.
In this scheme, D must be the number of scatterers, and in practical applications, for example, the Akaike's Information Criteria (AIC) or the Minimum Description Length (MDL) criteria are used to determine D.

In this study, in order to avoid artifacts through periodicity, we randomly changed the transmission wave frequency. With K transmissions having a randomly shifted frequency band, we estimate $\boldsymbol{R}$ as an ensemble average of $\hat{\boldsymbol{R}} = (\sum_{k=1}^{K} \boldsymbol{z}\boldsymbol{z}^{\mathrm{H}})/K$.

2.2 Synthetic Aperture-SCM

The SCM performs super-resolution processing for each imaging line. For that purpose, it is necessary to transmit multiple FM chirp pulses having different frequency bands in each direction corresponding to each imaging line; see Fig. 3 (a). If the image consists of N lines and K times of transmissions are performed in each direction, $N \times K$ transmissions must be made to generate the whole image. This extremely decreases the frame rate when super-resolution is performed on the entire imaging area. In order to solve the problem, the SA-SCM is realized by incorporating the SAI (Synthetic Aperture Imaging) into the SCM. In the SAI, unfocused pulses are transmitted in a wide range from sub-aperture elements [Fig. 3 (b)], and for each transmission, echoes from the entire imaging area are received simultaneously by all the elements and receive beam forming is applied. By randomly changing the frequency band of each transmitted FM-chirp pulse in the SAI, the total number of the transmissions is reduced. The above-mentioned $N \times K$ times of transmission in the SCM is realized by only K transmissions in the SA-SCM. Multiple line signals with different frequencies for each line are input to the SCM process. To avoid frequency deviation related to the position of the sub-aperture for transmission, a frequency band is randomly assigned to the position of the sub-aperture.

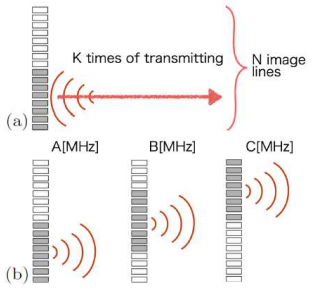

Figure 3: Transmission procedure: (a) SCM; (b) SA-SCM.

2.3 SCM-Weighted SA

Since the SCM is executed for each image line, discontinuities tend to occur in the lateral direction. In order to solve the problem, we proposed a new DAS incorporating the SCM results. In this method, the SCM is firstly applied to the echoes received by each element before the DAS processing. Although it is possible to apply the DAS to the SCM result, i.e., $S(t)$ defined by Eq. 10, since $S(t)$ does not include phase information, suppression of unwanted signals using phase mismatch is not done. By multiplying the received RF echo of each element by $S(t)$, we improve the range resolution of echo before the DAS beamforming and generate an image by the DAS. We call this method the SCM-weighted SA. Therefore, an image can be obtained for each frequency of the transmission pulse, and it can be used as multispectral information, or by integrating all of them, an image with high SNR can be obtained while avoiding grating lobes.

In this method, unlike the SA-SCM, it is necessary to fix transmission positions of plural transmissions to the same one in the array transducer. If the transmission of different frequencies is performed from different positions, the time position of the corresponding reflected wave will deviate between the echoes used for the SCM processing, and hence, the SCM processing can not be executed correctly. This limitation is not a problem for phased array transducers. However, in linear arrays and convex arrays, this limitation is not desirable in order to properly measure the information of the entire imaged area. In order to avoid this problem, it is sufficient to execute the SCM-weighted SA for some transmission positions, and to do so, apply a method based on the concept of compressive sensing in (Liu et al., 2018) to reduce the transmission position is effective.

2.4 High Range-Resolution FDMAS

In this section, we propose the FDMAS in baseband and a new beamformer with improved its range resolution. In the SCM-weighted SA, the first SCM processing uses the pulse-compressed IQ (In-phase and Quadrature-phase) echoes, whereas the subsequent DAS beamforming is applied to the pulse-compressed RF echo, and finally in order to generate the B-mode image. Namely, the beamformed RF signal is converted to the IQ signal again. Since this series of procedures is inefficient, the FDMAS should be realized in baseband when incorporating the SCM results into the FDMAS.

In the baseband FDMAS, first, time delay of the pulse-compressed IQ echo is corrected instead of the RF echo. In addition, it is necessary to compensate the phase deviation of the IQ signal, which is caused by the time delay correction. The correction amount is calculated by the following equation.

$$E(n) = \exp(i\beta n^2), \tag{11}$$

where β satisfies the relation $\beta = \pi d^2/(\lambda R_0)$, d is the pitch between transducer elements, R_0 is the shortest distance from the transducer array to the targeted imaging point and n is a number corresponding to each element of the transducer. The value of n at the shortest distance from the imaging point is set to 0. The phase is corrected by multiplying the analytic representation of the delay-corrected received echoes by Eq. 11. Figure 4 shows an example of the real part of Eq. 11 corresponding to the certain position in the image. For the setting of Fig. 4, d is set to 0.14 mm, λ is set to 0.3 mm, R_0 is set to 15 mm and the center element of the sensor array holds $n = 0$. This phase correction corresponds to Doppler compression processing in synthetic aperture radar and β is called Doppler constant. In the DAS, delay-corrected received echoes received by all elements are added up, but in the FDMAS, corrected received echoes are multiplied by a combination of all pairs and added. Assuming that the number of elements used for beamforming is N, the number of all combinations of the pairs is

$$\binom{N}{2} = \frac{N^2 - N}{2}. \tag{12}$$

Physical dimension is changed by multiplication, and therefore processing to restore the dimension is performed. That is

$$\hat{s}_{ij}(t) = \mathrm{sign}\left(s_i(t)s_j(t)\right)\sqrt{|s_i(t)s_j(t)|}, \tag{13}$$

where s_i indicates the IQ signal (complex number) of the ith element and $\mathrm{sign}(x)$ represents a unit complex number corresponding to x. The correlation of two complex signals is generally computed as a complex conjugate product, that indicates $s_i(t)^{\mathrm{H}}s_j(t)$ in this case. However, it was experimentally confirmed that it is difficult to detect the phase difference between

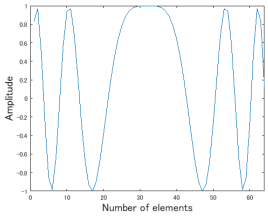

Figure 4: Example of real pert of Equation 1 at the certain position in image.

two signals with little time lag when using $s_i(t)^{\mathrm{H}} s_j(t)$. On the other hand, if $s_i(t)$ and $s_j(t)$ are target signals without time lag, the product $s_i(t)s_j(t)$ becomes a complex number of the same argument in all element pairs, and a large signal can be obtained by adding them together. For pairs with time lags, we found that the difference in argument is emphasized, especially for irregular signals such as speckle, the randomness of the argument is strongly generated, and cancellation occurs by adding them together. Therefore, in our method, we adopt $s_i(t)s_j(t)$ for multiplying processing. It is noted that $|s_i(t)s_j(t)| = |s_i(t)^{\mathrm{H}} s_j(t)|$.

In the original FDMAS, $s_i(t)$ in Eq. 13 is a real number (RF signal), and Eq. 13 in this study is a complex version of the original equation of the FDMAS. From these equations, the signal after the addition is

$$y^*_{DMAS}(t) = \sum_{i=1}^{N-1} \sum_{j=i+1}^{N} \hat{s}_{ij}(t) = \sum_{n=1}^{(N^2-N)/2} \hat{s}_n(t). \quad (14)$$

The B-mode image can be generated by computing the amplitude of the complex value $y^*_{DMAS}(t)$. In the FDMAS in RF band, it is necessary to extract the band corresponding to the frequency twice the frequency band of the transmission wave by using the band pass filter. On the other hand, in the FDMAS in baseband, the low pass filter is adopted instead of the band pass filter, since both fundamental and 2nd harmonic components of the result of Eq. 14 appear around a DC component. This means that the fundamental and the 2nd harmonic components are simultaneously extracted and used for imaging, what is expected to improve the SNR.

In order to improve the range resolution of the original FDMAS, we adopt the same method in the SCM-weighted SA to incorporate the SCM result into the FDMAS. Namely, before the processing of Eq. 14, $s_i(t)$ is multiplied by the corresponding $S(t)$ obtained by applying the SCM to the echoes before beamforming. We call this new beamformer HRR-FDMAS (High Range-Resolution FDMAS). The restriction of pulse transmission position exists similarly to the SCM-weighted SA, and its improvement strategy is the same as the SCM-weighted SA, and it will be a future task.

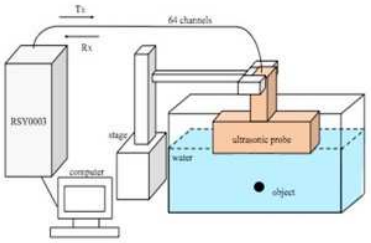

Figure 5: Experiment setting using metal wire with vinyl coating.

3 EXPERIMENT

3.1 Experiment Conditions

In the experiments, the transmission and reception sequences were generated using an experimental platform for medical ultrasound (RSYS0003, Microsonic Inc., Japan) with a sampling rate of 31.25 MHz. The number of transducer elements used for both transmission and reception is 64, while the element pitch is 0.315 mm. Transmitted waves are restricted to seven gradations. A linear array probe (T0-1599, Nihon Dempa Kogyo Co., Ltd., Japan) was also used. This probes center frequency is 7.5 MHz and its specific bandwidth is 70%. The signal processing required was performed offline using MATLAB software.

3.2 Experiments Using Wire Target

Figure 5 shows the experiment setting. We performed an experiment using a vinyl coated metal wire with a diameter of 1.5 mm that was placed in the water at a distance of 10 mm from the transducer as an imaging target. The divergent waves were transmitted using a central sub-array composed of 8 elements with a focal point of -0.63 mm with respect to the sub-array width of 2.52 mm. Because the probe element spacing is wider, it is likely that grating lobes will be formed. The frequency band of the FM chirp pulse that is used in the experiment is set at a relatively narrow 2 MHz, as described in the Table 1. Although the frequency band that is used is not the most effective band for all the transmissions, it was confirmed that can be performed appropriately.

3.3 Performance Evaluation of Baseband FDMAS

First, performmance comparison between the DAS and the FDMAS were conducted. Figure 6 shows the B-mode images of processing in baseband, and Fig. 7

Table 1: Parameter settings of the transmitted FM-chirp pulse.

Parameter	Value
Frequency band width	2 MHz
Chirp pulse duration	5 μs
Variation range of center freq.	4 to 6 MHz
Number of transmission	15
Apodization	Hanning window

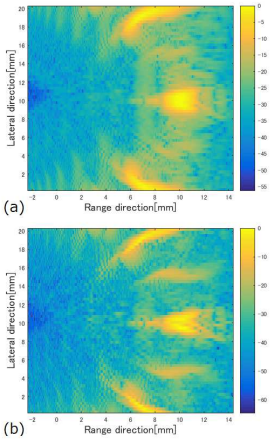

Figure 6: B-mode images using 4.62 MHz: (a) baseband DAS; (b) baseband FDMAS.

shows the intensity distribution profiles on a line crossing the imaging target. Since the reception echoes of a plurality of frequencies are obtained for the SCM processing, it is possible to generate a B-mode image using each frequency echo. In this study, the lowest frequency of 4.62 MHz was used for imaging to avoid grating lobes as much as possible. In order to confirm that the grating lobes increase by using the high frequency echo for B-mode imaging, the baseband FDMAS result using high frequency of 5.75 MHz is shown in Fig. 8(a). In addition, the intensity distribution profiles in the lateral direction using 4.62 MHz and 5.75 MHz are shown in Fig. 8(b). From Figs. 6 and 7, it can be confirmed that the range resolution almost unchanged, but the lateral resolution improves when the FDMAS is applied.

Next, in order to evaluate the performance of the baseband FDMAS, the SNR was compared with the RF band FDMAS. Figure 9 shows the B-mode image of the RF band FDMAS and Fig. 10 shows the intensity distribution profiles on a line crossing the imaging target. In the definition of the SNR, the peak of the echo signal from the target was adopted as the signal intensity, and the noise average was adopted as the noise intensity in the range direction profile of one line where the target exists. The SNR was 32.63 dB for RF band FDMAS and 37.12 dB for baseband FDMAS. From this result, it was confirmed that the ba-

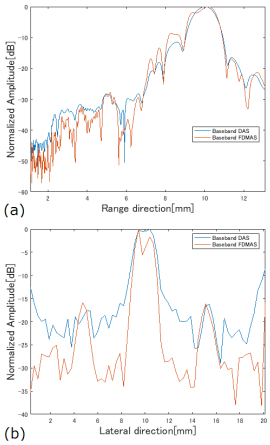

Figure 7: Intensity distribution profiles on a line crossing imaging target using 4.62 MHz: (a) range direction; (b) lateral direction.

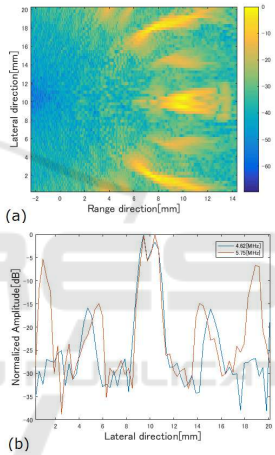

Figure 8: Grating lobes increase using high frequency echo: (a) B-mode image using 5.75 MHz; (b) intensity distribution profiles in lateral direction using different frequencies.

seband FDMAS improves the SNR and the lateral resolution. In the RF band FDMAS, the range resolution is improved by extracting the double frequency band using a band pass filter. On the other hand, the baseband FDMAS processes the baseband signal in which both the transmission frequency component and the doubled frequency component are converted, so that the SNR can be improved. By using not only the double frequency band but also the transmission frequency band, we were worried about lowering the resolution compared to the FDMAS in the RF band. However, due to the fact that the double frequency band has sufficient power, no reduction in range resolution was confirmed. Improvement of lateral resolution is considered to be due to phase matching of processing in baseband. However, processing with baseband causes artifacts regardless of the beamforming method. Since this does not occur in processing

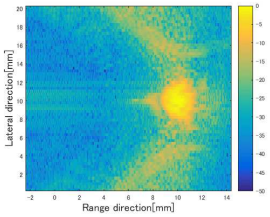

Figure 9: B-mode image of RF band FDMAS.

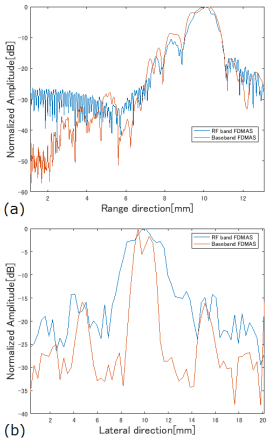

Figure 10: Intensity distribution profiles on a line crossing imaging target of B-mode images in RF band and baseband FDMAS: (a) range direction; (b) lateral direction.

with the RF band, we will investigate the cause in the future.

3.4 Performance Evaluation of HRR-FDMAS

Performance of HRR-FDMAS was evaluated. Figure 11 shows the B-mode images by the SCM-weighted SA and by the HRR-FDMAS, and Fig. 12 shows the intensity distribution profiles on a line crossing the imaging target of all the methods described in this paper. In this experiment, the value of D in SCM processing was set to 1 because there is only one target. Figure 13 shows the result of SCM when changing the value of D. As shown in Fig. 13, artifacts may be generated in the result of the SCM if D setting is not appropriate. From this result, it can be confirmed that the HDD-FDMAS improves the lateral resolution compared with the SCM-weighted SA.

4 CONCLUSION

We first proposed the realization of FDMAS in baseband, and experimentally confirmed that SNR and lateral resolution are greatly improved compared with

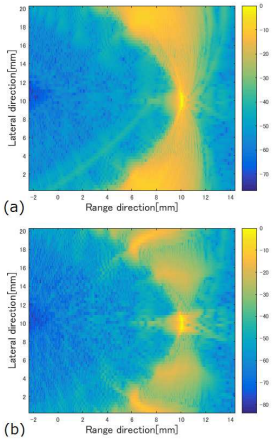

Figure 11: B-mode images: (a) SCM-weighted SA; (b) HRR-FDMAS.

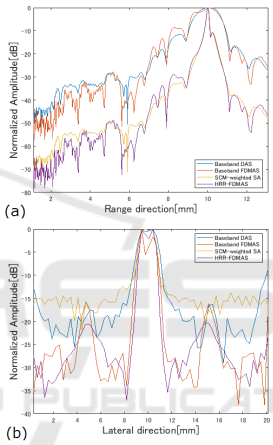

Figure 12: Intensity distribution profiles on a line crossing imaging target of all methods described in this paper: (a) range direction; (b) lateral direction.

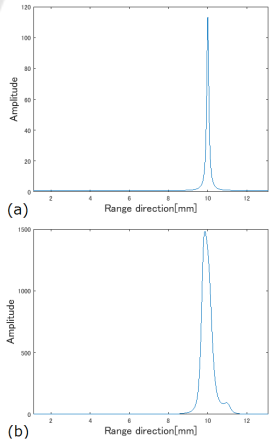

Figure 13: Result of SCM when changing the value of D: (a) $D = 1$; (b) $D = 5$.

FDMAS in RF band. Subsequently, we proposed a new beamformer HRR-FDMAS in which the SCM result is applied to the FDMAS in order to improve range resolution. The improvement of the spatial resolution for the FDMAS in the conventional RF band was clearly confirmed by experiments. Evaluation and verification of actual performance of the HRR-FDMAS for living organisms is a task to be carried out as soon as possible in the future.

In the HRR-FDMAS, the SCM processing takes much computational cost because the phase information of the carrier is extracted by the MUSIC algorithm that requires the eigenvalue analysis. Therefore, we are considering improving the range resolution by other methods that can use phase information with a low cost procedure. The essence of the SCM is to transmit and receive multiple times while changing the carrier frequency irregularly, and we aim to propose an efficient beamforming method that can take advantage of this principle.

REFERENCES

Amy, D., Durante, E., and Tot, T. (2015). The lobar approach to breast ultrasound imaging and surgery. *Ultrasonics*, 42(3):331–339.

Fujiwara, M., Okubo, K., and tagawa, N. (2009). A novel technique for high resolution ultrasound imaging using super resolution fm-chirp correlation method (scm). In *Proc. IEEE Int. Ultrason. Symp.*, pages 2390–2393.

Hazas, M. and Hopper, A. (2006). Broadband ultrasonic location systems for improved indoor positioning. *IEEE Trans. Mobile Computing*, 5(5):536–547.

Holm, S., Synnevdg, J. F., and Austeng, A. (2009). Capon beamforming for active ultrasound imaging systems. In *Proc. IEEE 13th DSP Workshop*, pages 60–65.

Jensen, J. A., Nikolov, S. I., Gammelmark, K. L., and Pedersen, M. H. (2006). Synthetic aperture ultrasound imaging. *Ultrasonics*, 44:e5–e15.

Liu, J., He, Q., and Luo, J. (2018). Compressed sensing based synthetic transmit aperture imaging: Validation in a convex array configuration. *IEEE trans. ultrason. ferroelectr. freq. control*, 65(3):300–315.

Matrone, G., Ramalli, A., Savoia, A. S., Tortoli, P., and Magenes, G. (2017). High frame-rate, high resolution ultrasound imaging with multi-line transmission and filtered-delay multiply and sum beamforming. *IEEE Trans. Med. Imag.*, 36(2):478–486.

Matrone, G., Ramalli, A., Tortoli, P., and Magenes, G. (2018). Experimental evaluation of ultrasound higher-order harmonic imaging with filtereddelay multiply and sum (f-dmas) non-linear beamforming. *Ultrasonics*, 86:59–68.

Matrone, G., Savoia, A. S., Caliano, G., and Magenes, G. (2015). The delay multiply and sum beamforming algorithm in ultrasound b-mode medical imaging. *IEEE Trans. Med. Imag*, 34(4):940–949.

Schmidt, R. O. (1986). Multiple emitter location and signal parameter estimation. *IEEE Trans. Antennas and Propagation*, 34(3):276–280.

Shoval, S. and Borenstein, J. (2001). Using coded signals to benefit from ultrasonic sensor crosstalk in mobile robot obstacle avoidance. In *Proc. IEEE Int. Conf. Robotics and Automation*, volume 3, pages 2879–2884.

Su, T., Li, D., and Zhang, S. (2018). An efficient subarray average delay multiply and sum beamformer algorithm in ultrasound imaging. *Ultrasonics*, 84:411–420.

Tagawa, N., Zhu, J., and Okubo, K. (2018). Performance analysis of high-frame rate and super-resolution ultrasound imaging based on frequency sweeping. *submitted to Applied Sciences*.

Thomenius, K. E. (1996). Evolution of ultrasound beamformers. In *Proc. IEEE Int. Ultrason. Symp.*, volume 2, pages 1615–1622.

Vignon, F. and Burcher, M. R. (2008). Capon beamforming in medical ultrasound imaging with focused beams. *IEEE trans. ultrason. ferroelectr. freq. control*, 24(10):1308–1322.

Wada, T., Ho, Y., Okubo, K., Tagawa, N., and Hirose, Y. (2015). High frame rate super resolution imaging based on ultrasound synthetic aperture scheme. *Physics Procedia*, 70:1216–1220.

Wang, Z., Li, J., and Wu, R. (2005). Time-delay- and time-reversal-based robust capon beamformers for ultrasound imaging. *IEEE Trans. Med. Imag.*, 24(10):1308–1322.

Ylitalo, J. (1996). A fast ultrasonic synthetic aperture imaging method: application to ndt. *Ultrasonics*, 34(2-5):331–333.

Zhou, L., Zhao, Y. J., and Cui, H. (2008). High resolution wideband doa estimation based on modified music algorithm. In *Proc. IEEE Int. Conf. Inf. Automat.*, pages 20–22.

Zhu, J. and Tagawa, N. (2018). Super-resolution ultrasound imaging based on the phase of the carrier wave without deterioration by grating lobes. In *Proc. Int. Conf. Pattern Recognition*, pages 2791–2796.